Contribution from the Dipartimento di Chimica Inorganica, Metallorganica ed Analitica, Università di Padova, 35131 Padova, Italy, Istituto di Chimica della Università della Basilicata, Potenza, Italy, Istituto di Teoria e Struttura Elettronica del CNR di Roma, Rome, Italy, and Anorganisch Chemisch Laboratorium, University of Amsterdam, Amsterdam, The Netherlands

Theoretical, UV-PES, XPS, and Mössbauer Investigation of the Electronic Structure of Dinuclear Metal Carbonyl Diimine Complexes with a Metallacyclopentadienyl System

R. Bertoncello,[1a] M. Casarin,*[,1a,b] M. Dal Colle,[1a] G. Granozzi,*[,1a] G. Mattogno,[1c] F. Muller,[1d] U. Russo,[1a] and K. Vrieze*[,1c]

Received May 22, 1989

The electronic structure of a series of metallacyclopentadienyl diiron complexes, containing a chelating 4e-donor 1,4-diaza-1,3-butadiene (R-DAB) ligand in different structural arrangements, is discussed by using SCF–first-principle discrete variational (DV)–Xα calculations and gas-phase UV-photoelectron (PE), solid-state X-ray PE (XPS), and Mössbauer spectroscopies. Comparison of the obtained theoretical results with those relative to the isoelectronic unsubstituted diiron metallacyclopentadienyl complex ($Fe_2(CO)_6(C_4H_4)$) indicates that, even though the substitution of two terminal CO ligands with R-DAB mainly affects molecular orbitals localized on the metal atom R-DAB is bonded to, the overall bonding scheme is significantly influenced by the coordination site of R-DAB. When compared to two carbonyls, R-DAB causes a higher amount of electronic density on the metal atom to which it is directly bonded. Moreover, the involvement of n^+ and n^- nitrogen lone-pair combinations in the metal–nitrogen interaction is computed to be definitely stronger than in complexes where R-DAB acts as a bridging 8e donor. Remarkable differences in structural data of the investigated series are discussed and clarified on the basis of the reported theoretical results. Transition-state ionization energies reproduce very well the experimental UV-PE pattern, allowing us to be confident about the main features of the bonding scheme. Furthermore, the computed different electronic charge distributions for the two nonequivalent iron sites along the series are well in tune with both Mössbauer experimental data and binding energy values obtained by XPS.

Introduction

Reactions of metal carbonyl complexes with α-diimines have in the past resulted in a very extensive chemistry.[2] The α-diimines show a versatile coordination behavior, and it has been found that the coordinated α-diimine ligand may easily participate not only in C–H and N–H bond formation[3,4] but also in C–C and N–C coupling reactions with a wide variety of unsaturated organic substrates, such as α-diimines,[5] carbodiimides (RN=C=NR),[6] sulfines (R_2C=S=O),[6] ketene (H_2C=C=O),[7] and alkynes (R′C≡CR″).[8] The substituted 1,4-diaza-1,3-butadiene (RN_α=$C_\beta H$–$C_\beta H$=$N_\alpha R$; hereafter R-DAB) shows several coordination modes, where it can act as a 2e (σ-N),[2] 4e (σ-N, σ-N′ chelating),[2] 4e (η^2-CN, η^2-CN′),[9] 2e, 2e (σ-N, σ-N′ bridging),[2] 6e (σ-N, μ_2-N′, η^2-CN′),[2] and 8e (σ-N, σ-N′, η^2-CN, η^2-CN′)[2] donor.

This paper is part of a systematic investigation of the electronic properties of dinuclear metallacycle complexes,[10] where the main aim is that of clarifying the bonding scheme within the metallacycle and the role played by the metal–metal bond in modifying metal–ligand interactions.[10a] Here we report a combined theoretical and experimental investigation of the electronic structure of a series of ferracyclopentadienyl diiron complexes ($Fe_2(CO)_4$(iPr-DAB)(C_4R_4)) obtained from the reactions of alkynes with metal carbonyl α-diimine complexes. Along the series the iPr-DAB (iPr = isopropyl) ligand is present in different structural arrangements (see I–III in Figure 1), as a result of steric properties of the alkynes.[11] The investigation has been carried out by combining SCF–first-principle discrete variational (DV)–Xα calculations with gas-phase UV photoelectron (PE), solid-state X-ray PE (XPS), and Mössbauer spectroscopies.

Quite recently some of us investigated, within the same theoretical framework, the electronic structure of the related molecules $Fe_2(CO)_6(C_4H_4)$[10a] (IV), $Ru_2(CO)_4$(R-DAB)(μ-CO)[10c] (V), and $Ru_2(CO)_4$(R-DAB)(μ-HC≡CH)[10c] (VI). In the following, an extensive use of comparisons with these theoretical results will be made in order to obtain a quantitative understanding of the different electronic behavior of the R-DAB ligand in different coordinative modes. Furthermore, such a comparison gives us the opportunity to go into the details of the Mössbauer spectrum of IV published more than 15 years ago.[12a,b]

Selected contour plots (CP's) of some molecular orbitals (MO's) important in describing the metal–ligand interactions are reported and discussed. Moreover, in order to facilitate the discussion of energy level distribution, we will make use of a density of states (DOS) analysis.

Experimental Section

Synthesis. The reported compounds were synthesized according to the published procedures.[11] After crystallization, their purity was checked by IR and ^{1}H NMR spectroscopies.

Theroetical Method. SCF Hartree–Fock–Slater (HFS)–discrete variational (DV)–Xα calculations[13] were performed on a VAX-8600 computer at the computing center of the University of Padova.

The approximations of the reported theoretical calculations are (i) the use of near-minimal atomic orbital (AO) basis sets, (ii) a SCC approx-

(1) (a) Università di Padova. (b) Università della Basilicata. (c) ITSEC, CNR. (d) University of Amsterdam.
(2) For recent review dealing with the chemistry of α-diimine ligands, see: Vrieze, K. *J. Organomet. Chem.* **1986**, *300*, 307 and references therein.
(3) Keijsper, J.; Grimberg, P.; van Koten G.; Vrieze, K.; Christophersen, M.; Stam, C. H. *Inorg. Chim. Acta* **1985**, *102*, 29.
(4) (a) Keijsper, J.; Mul, J.; van Koten, G.; Vrieze, K.; Ubbels, H. C.; Stam, C. H. *Organometallics* **1984**, *3*, 1732. (b) Zoet, R.; van Wijnkoop, M.; Versloot, P.; van Koten, g.; Vrieze, K. *Organometallics*, in press.
(5) (a) van Koten, G.; Jastrzebski, J. T. B. H.; Vrieze, K. *J. Organomet. Chem.* **1983**, *250*, 49. (b) Staal, L. H.; Oskam, A.; Vrieze, K.; Roosendaal, E.; Schenk, H. *Inorg. Chem.* **1979**, *18*, 1634. (c) Staal, L. H.; Polm, L. H.; Balk, R. W.; van Koten, G.; Vrieze, K.; Brouwers, A. M. F. W. *Inorg. Chem.* **1980**, *19*, 3343. (d) Polm, L. H.; van Koten, G.; Elsevier, C. J.; Vrieze, K.; van Santen, B. F. K.; Stam, C. H. *J. Organomet. Chem.* **1986**, *304*, 353.
(6) Keijsper, J.; Polm, L. H.; van Koten, G.; Vrieze, K.; Schagen, J. D.; Stam, C. H. *Inorg. Chim. Acta* **1985**, *103*, 137.
(7) Polm, L. H.; van Koten, G.; Vrieze, K.; Stam, C. H.; van Tunen, W. C. J. *J. Chem. Soc., Chem. Commun.* **1983**, 1177.
(8) Staal, L. H.; van Koten, G.; Vrieze, K.; van Santen, B. F. K.; Stam, C. H. *Inorg. Chem.* **1981**, *20*, 3598.
(9) Kokkes, M. W.; Stufkens, D. J.; Oskam, A. *J. Chem. Soc., Dalton Trans.* **1984**, 1005.
(10) (a) Casarin, M.; Ajò, D.; Vittadini, A.; Ellis, D. E.; Granozzi, G.; Bertoncello, R.; Osella, D. *Inorg. Chem.* **1987**, *26*, 2041. (b) Casarin, M.; Ajò, D.; Granozzi, G.; Tondello, E.; Aime, S. *Inorg. Chem.* **1985**, *24*, 1241. (c) Casarin, M.; Vittadini, A.; Vrieze, K.; Muller, M.; Granozzi, G.; Bertoncello, R. *J. Am. Chem. Soc.* **1988**, *110*, 1775.
(11) (a) Muller, F.; Han, I. M.; van Koten, G.; Vrieze, K.; Heijdenrijk, D.; de Jong, R. L.; Zoutberg, M. *Inorg. Chim. Acta* **1989**, *158*, 81. (b) Muller, F. Ph.D. Thesis, Amsterdam, 1988.
(12) (a) Herber, R. H.; King, R. B.; Wertheim, G. K. *Inorg. Chem.* **1964**, *3*, 101. (b) King, R. B.; Epstein, L. M.; Gowling, E. W. *J. Inorg. Nucl. Chem.* **1970**, *32*, 441. (c) Emerson, G. F.; Mahler, J. E.; Pettit, R.; Collins, R. *J. Am. Chem. Soc.* **1964**, *86*, 3590. (d) Collins, R.; Pettit, R. *J. Am. Chem. Soc.* **1963**, *85*, 2332. (e) Greenwood, N. N.; Gibb, T. C. In *Mössbauer Spectroscopy*; Chapman and Hall: London, 1971; p 227.
(13) (a) Averill, F. W.; Ellis, D. E. *J. Chem. Phys.* **1973**, *59*, 6412. (b) Rosen, A.; Ellis, D. E.; Adachi, H.; Averill, F. W. *J. Chem. Phys.* **1976**, *65*, 3629 and references therein. (c) Trogler, W. C.; Ellis, D. E.; Berkowitz, J. *J. Am. Chem. Soc.* **1979**, *101*, 5896.

0020-1669/89/1328-4243$01.50/0 © 1989 American Chemical Society

Table I. Atomic Character from the SCC DV-Xα Calculation for $Fe_2(C_4H_4)(Me\text{-}DAB)(CO)_4$ (I)

MO	eigenvalue, $-E$, eV	TSIE, eV	population, % Fe s	Fe p	Fe d	Fe' s	Fe' p	Fe' d	$(CO)_{sb}$	3 CO	DAB	C_4H_4	character
34a'[a]	3.35		0	-1	19	0	1	8	3	4	63	3	π_3^* DAB
33a'	4.79	7.56	0	0	90	0	0	1	0	2	3	4	
22a''	5.11	7.88	0	0	61	0	2	8	1	12	9	7	
32a'	5.45	8.22	1	5	37	0	0	13	6	6	27	5	3d-like MO's +
31a'	6.34	9.11	1	2	25	0	4	26	1	16	3	22	π_3^* DAB +
21a''	6.60	9.37	0	1	8	0	3	48	10	11	4	15	π_3^* C_4H_4
30a'	6.70	9.47	0	1	5	0	2	54	6	19	2	11	
29a'	6.82	9.59	0	1	3	0	5	55	6	19	0	11	
20a''	7.45	10.22	0	2	3	0	0	21	1	9	9	55	π_2 C_4H_4
19a''	7.71	10.48	0	1	2	0	0	0	0	8	81	7	
18a''	8.21	10.98	0	2	8	0	3	6	4	3	16	58	$n^-_{C_4H_4} + n^-_{DAB}$
28a'	8.74	11.51	0	4	5	0	2	9	4	4	33	39	
27a'	9.36	12.13	0	0	1	0	0	3	2	21	15	58	π_1 C_4H_4
17a''	9.46	12.23	0	0	25	0	0	0	0	8	59	8	$n^-_{DAB} - n^-_{C_4H_4}$
26a'	9.82	12.59	2	0	11	0	0	4	1	22	30	30	

[a] Lowest unoccupied MO.

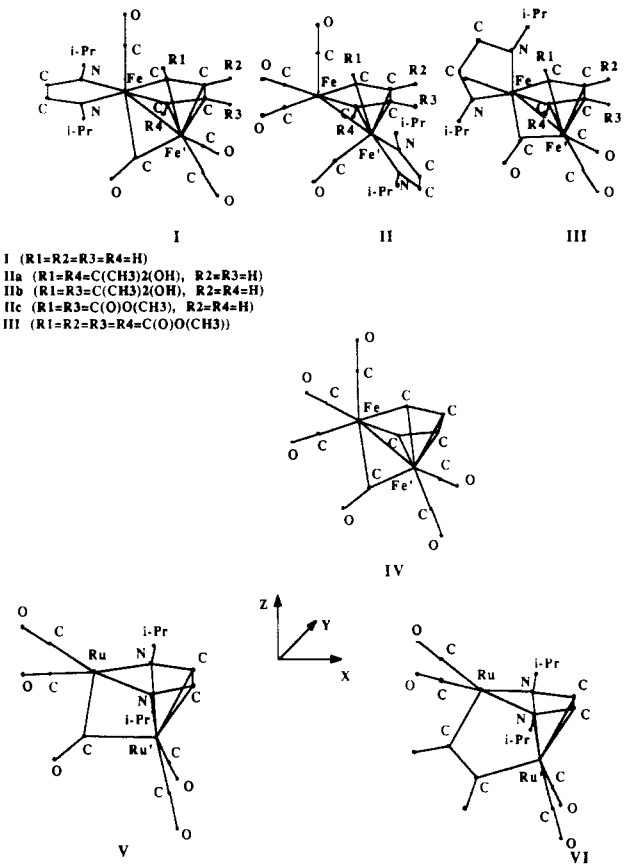

I (R1=R2=R3=R4=H)
IIa (R1=R4=C(CH3)2(OH), R2=R3=H)
IIb (R1=R3=C(CH3)2(OH), R2=R4=H)
IIc (R1=R3=C(O)O(CH3), R2=R4=H)
III (R1=R2=R3=R4=C(O)O(CH3))

Figure 1. Schematic views of investigated molecules. The reference framework is also given.

imation of the Coulomb potential, representing atoms by overlapping spherical charge distributions,[13b] (iii) the use of the Gaspar–Kohn–Sham exchange potential,[14] (iv) neglect of relativistic effects, and (v) Slater's transition-state (TS) formalism[15] to calculate the ionization energies (IE's). Numerical AO's (through 4p on Fe, 2p on C, N, and O, and 1s on H) obtained for the neutral atoms were used as basis functions. Due to the size of the investigated systems, orbitals 1s–3p (Fe) and 1s on carbon, nitrogen, and oxygen were treated as a part of a frozen core in the molecular calculations. Gross atomic charges and bond overlap populations (OP's) were computed by using Mulliken's scheme.[16] The experimental geometry[11] of I was idealized to C_s symmetry for use in the calculations (see Figure 1). In order to save computer time, the electronic properties of the R-DAB substituents (R = isopropyl) have been simulated by replacing them with methyl groups. Moreover, despite the lack of any symmetry element in the solid-state structure of compound II,[11] a SCC ground-state calculation on a prototype molecule with the R-DAB bonded to Fe'[17] has been run to investigate, at least semiquantitatively, differences in relative bonding schemes. The MO's have then been labeled according to the irreducible representations a' and a''.[18] Instead of the eigenvalues being displayed along an energy axis, the density of states (hereafter DOS) has been plotted as a function of energy. The component, or partial, density of states function (PDOS) for atomic basis function j is constructed according to the published procedure.[19] These plots have an advantage over molecular energy level schemes because they provide insight into the disposition and composition of orbitals over a broad range of energy.

UV Photoelectron Spectra. He I and He II excited PE spectra were measured on a Perkin-Elmer PS-18 spectrometer modified for He II measurements by inclusion of a hollow-cathode discharge lamp giving high output of He II photons (Helectros Developments). The ionization energy (IE) scale was calibrated by reference to peaks due to admitted inert gases (Xe–Ar) and to the He $1s^{-1}$ self-ionization. A heated inlet probe system was adopted at 90–110 °C.

X-ray Photoelectron Spectra. X-ray photoelectron spectra were recorded with a Vacuum Generator Ltd. ESCA 3 MK II spectrometer using Al $K\alpha_{1,2}$ excitation (1486.6 eV) at a residual pressure of 10^{-7} Pa. Samples were dusted as a thin film over a gold plate to minimize charging effects. Calibration was made by the $4f_{7/2}$ gold signal at 83.7 eV. Sample charging was corrected by referencing to the C_{1s} line of carbon in the contaminating oil, taken at 285.0 eV. The accuracy of the measured binding energy was estimated at ±0.2 eV. Throughout XPS measurements the samples were cooled to liquid-N_2 temperature to prevent secondary decomposition effects. Peak deconvolution was performed with a Du Pont 310 curve resolver using a Gaussian shape fit.

Mössbauer Spectra. Mössbauer-effect spectra were obtained on a conventional constant-acceleration spectrometer that utilized a room-temperature rhodium matrix cobalt-57 source. It was calibrated at room temperature with natural-abundance α-iron foil. The spectra were fitted to Lorentzian line shapes by using standard least-squares computer minimization techniques. The error analysis was carried out by using error propagation techniques. All the components of each spectrum were allowed to vary as symmetric doublets until the best fit was obtained.

Results and Discussion

Theoretical Results. Molecular systems I and IV are very similar indeed: they differ only in the substitution of two carbonyls

(14) (a) Gaspar, R. *Acta Phys. Acad. Sci. Hung.* **1954**, *3*, 263. (b) Kohn, W.; Sham, L. J. *Phys. Rev.* **1965**, *140A*, 1133.
(15) Slater, J. C. *Quantum Theory of Molecules and Solids. The Self-Consistent Field For Molecules and Solids*; McGraw-Hill: New York, 1974; Vol. 4.
(16) Mulliken, R. S. *J. Chem. Phys.* **1955**, *23*, 1833.
(17) In such a calculation a perfectly planar $Fe(CO)_2(C_4H_4)$ unit, with the same Fe(CO) and $Fe(C_4H_4)$ mean bond distances of I, is bonded to a Fe'(CO)(R-DAB) fragment, where no semibridging carbonyl is assumed.
(18) Symmetry properties of I and II are herein described by the C_s symmetry point group. The a' and a'' MO labeling allows us to distinguish π_3^* and/or π_1 (both a' in symmetry) from π_2 (a'') involvement in the metal–(C_4H_4) interaction.
(19) Holland, G. F.; Ellis, D. E.; Trogler, W. C. *J. Am. Chem. Soc.* **1986**, *108*, 1884.

Table II. Atomic Character from the SCC DV-Xα Calculation for Fe(Me-DAB)CO

MO	eigenvalue, $-E$, eV	population, % Fe s	Fe p	Fe d	CO	2 N	2 C	2 CH_3	2 H	character[a]
11a''[b]	2.24	0	19	65	3	9	0	3	1	
16a'	2.69	1	16	39	6	22	12	4	0	$d_{xz} + \pi_3^*$
15a'	3.15	0	0	96	0	0	1	3	0	
10a''	3.75	0	0	70	18	3	8	1	0	3d-like MO's
14a'	4.11	0	0	65	17	7	10	1	0	
9a''	6.12	0	0	4	5	57	21	13	0	π_2
8a''	7.44	0	0	18	4	53	3	15	7	n^-
13a'	7.69	0	1	11	9	43	12	13	9	n^+
12a'	8.41	1	0	0	31	13	46	8	1	π_1
7a''	8.78	0	0	3	93	2	0	2	0	$\pi_\parallel$ CO
11a'	8.89	1	0	4	92	1	2	0	0	5σ CO

[a] $\parallel$ refers to the xy plane. [b] Lowest unoccupied MO.

Table III. Atomic Character from the SCC DV-Xα Calculation for $Fe(CO)_3$

MO	eigenvalue, $-E$, eV	population, % Fe s	Fe p	Fe d	3 CO	character[a]
13a'	3.43	18	41	17	24	
12a'[b]	4.38	0	30	45	25	
8a''	4.41	0	31	48	21	
7a''	6.26	0	0	68	32	3d-like MO's + π^*
11a'	6.28	0	0	68	32	
10a'	6.31	0	0	64	35	
6a''	9.64	0	0	0	100	73% π $CO_\parallel$ + 27% π $CO_\perp$
9a'	9.76	0	0	6	94	49% π $CO_\parallel$ + 45% π $CO_\perp$
5a''	9.77	0	0	4	96	83% 5σ $CO_\parallel$ + 13% 5σ $CO_\perp$
8a'	10.53	0	0	5	95	86% 5σ $CO_\perp$
4a''	10.62	0	0	11	89	23% π $CO_\perp$ + 66% π $CO_\parallel$
7a'	10.75	0	0	8	92	92% 5σ $CO_\parallel$

[a] $\perp$ and $\parallel$ refer to xy plane. [b] Lowest unoccupied MO.

bonded to Fe for R-DAB. In this respect, Muller et al. have anticipated, on qualitative grounds, the different electronic behavior of R-DAB compared to that of two carbonyls in a contribution dealing with syntheses, reactivities, and solid-state structures of the title molecules.[11a] The importance of testing quantitatively their predictions is quite obvious. On this basis, we decided to carry out a series of ground-state DV-Xα calculations on the electronic structure of I and of the fragments Fe(CO)(R-DAB) and $Fe(CO)_3$. Charge density analyses of the relative outermost MO's are reported in Tables I–III, respectively; in Table IV selected orbital occupation numbers and overlap populations (OP's) are collected, while in Figure 2 energy levels pertaining to the two fragments are compared.

The electronic structure of I can be usefully analyzed by focusing our attention on a series of local interactions, namely (i) Fe–(R-DAB), (ii) Fe–(C_4H_4), (iii) Fe′–(C_4H_4), and (iv) Fe–Fe′.

The first point deserves particular attention because it gives us the opportunity to study both the perturbations induced in IV by replacing two terminal carbonyls with R-DAB and the different electronic behavior of R-DAB in the complex I (a σ-N, σ-N′ chelating 4e donor) and in V and VI (a σ-N, σ-N′, η^2-CN, η^2-CN′ bridging 8e donor) complexes.[10c] The former can be easily worked out by making reference to Tables II–IV and to Figure 2. The outstanding feature of this figure is obvious: as one passes from $Fe(CO)_3$ to Fe(CO)(R-DAB) there is an overall shift of the electronic levels toward higher energy. Such an effect is the consequence of two different factors, namely (a) the better energy matching between d AO's and in-phase and out-of-phase linear combinations of nitrogen lone pairs (n^+ and n^-, respectively) compared to that between d AO's and carbonyl-based 5σ levels (compare in Tables II and III the different iron participation in MO's mainly n^+, n^-, and 5σ in character) and (b) the poorer π-acceptor capability of R-DAB vs that of CO's. Point b is a problem because it is counterintuitive. Actually, the energy matching between metal-based orbitals and the π_3^* R-DAB level is definitely better than that with CO-based π^* orbitals; nevertheless, we have to remember that π_3^* is the only accessible R-DAB virtual level at variance with carbonyls, which, as a whole, have four empty π^* orbitals, two parallel and two perpendicular to the xy plane (in our framework). In conclusion, the analysis of theoretical and data relative to Fe(CO)(R-DAB) and $Fe(CO)_3$ points out that the substitution of two carbonyls with R-DAB gives rise to a higher charge density on the metal atom (see different iron charges in Table IV), in agreement with previous qualitative predictions.[11a]

If we go on with a comparison between I and IV and keep in mind what has been just reported about the electronic structure of $Fe(CO)_3$ and Fe(CO)(R-DAB), it turns out that an important difference between I and IV is the nitrogen-induced charge accumulation on the Fe atom, which will partially overcome its

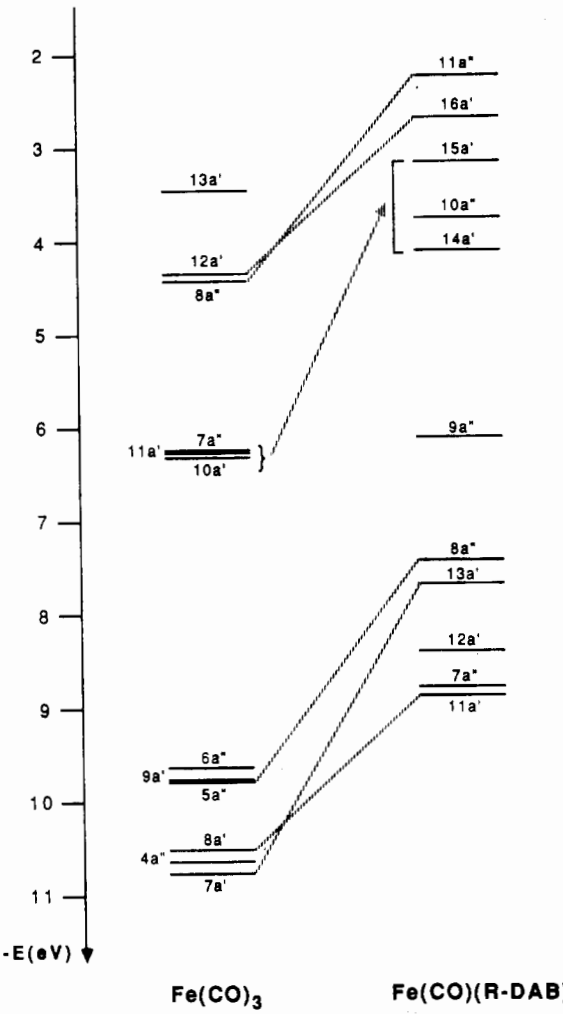

Figure 2. Comparison of the energy levels for $Fe(CO)_3$ and Fe(CO)(R-DAB) fragments.

Table IV

Selected Orbital Occupation Numbers

I

	Fe	Fe′		C_α	C_β	C_β^{DAB}	N_α	C_{sb}
3d	6.47	6.51						
4s	0.13	0.05	2s	1.42	1.18	1.08	1.57	1.36
4p	0.32	0.37	2p	3.26	3.09	3.09	3.72	2.76
Q	1.08	1.07		−0.68	−0.27	−0.16	−0.29	−0.12

Fe(CO)(R-DAB)

	Fe		C_β^{DAB}	N_α	$C_{carbonyl}$
3d	6.58				
4s	0.21	2s	1.06	1.55	1.36
4p	0.34	2p	3.07	3.81	2.78
Q	0.87		−0.13	−0.36	−0.14

$Fe(CO)_3$

	Fe		$C_{carbonyl}$
3d	6.56		
4s	0.03	2s	1.37
4p	0.47	2p	2.75
Q	0.94		−0.12

$Fe_2(CO)_4(C_4H_4)$(R-DAB)[a]

	Fe	Fe′		C_α	C_β	C_β^{DAB}	N_α
3d	6.51	6.42					
4s	0.10	0.17	2s	1.42	1.17	1.06	1.57
4p	0.39	0.37	2p	3.26	3.11	3.08	3.69
Q	1.00	1.04		−0.68	−0.28	−0.14	−0.26

Selected Overlap Populations

	Fe–Fe′	Fe–C_α	Fe–N_α	Fe–C_α	Fe–C_β	Fe–C_{sb}	Fe–C_{sb}	N_α–C_β	C_α–C_β	Fe–$C_{carbonyl}$
I	0.03	0.53	0.44	0.19	−0.12	0.13	0.18	0.95	0.86	
Fe(CO)(R-DAB)			0.55					0.84		
$Fe(CO)_3$										0.60
$Fe_2(CO)_4(C_4H_4)$(R-DAB)[a]	0.13	0.48	0.42[b]	0.22	−0.25			0.96	0.87	

[a] II-like prototype molecule. [b] Fe′–N_α.

"unsaturation".[20] On this basis, we can anticipate a less important role in I of the Fe′→Fe dative bond invoked by Cotton,[21] within a valence bond (VB) description of the electronic structure of IV, in order to allow the fulfillment of the EAN (effective atomic number) rule[22] for both iron atoms. The comparison of the electronic structures of I and IV provides us with another relevant indication; i.e. even though the Fe-localized MO's undergo significant perturbations on substituting two carbonyls with R-DAB, those mainly Fe′ in character do not. Actually, the three Fe′ d pairs (21a″, 30a′, 29a′ MO's) are grouped in a very narrow energy range (6.60–6.80 eV), similar to the case for IV and for Fe-$(CO)_3(\eta^4\text{-}C_4H_6)$[10a] (VII); furthermore, their energy position is exactly the same as in VII,[10a] giving support to the absence of an *effective* Fe′→Fe dative bond, which would have shifted the Fe′-localized MO's toward lower energies because of the formal +1 charge carried by Fe′.[21]

As far as the electronic behavior of R-DAB is concerned, we can say that the main difference between the 4e- and 8e-donor coordination modes is related to the involvement of n^+ and n^- combinations in the metal–nitrogen interaction being stronger in I than in V and VI.[10c] This difference has to be associated with the strong $\pi_2 \rightarrow$ Ru′ donation in V and VI, which shifts the n^+ and n^- combinations toward lower energies, reducing, as a consequence, the energy matching with Ru 4d AO's. The same comparison gives us another important possibility, i.e. the role played by M → π_3* back-donation and $\pi_2 \rightarrow$ M′ donation[23] in lengthening the N_α–C_β bond. This has to be done with the reminder that, on passing from 4e- to 8e-donor behavior, it is more important to analyze the variations undergone by the N_α–C_β bond length than by the C_β–C_β ones, both π_3* and π_2 levels being mainly localized on the N_α atoms.[10c] Now, if we compare the N_α–C_β (C_β–C_β) bond lengths in the free ligand (1.258 Å (1.42) Å)),[24] in I (1.30 Å (1.404 Å)),[11] and in V and VI (1.457 Å (1.40 Å)),[25] we could suggest that donation plays a more important role than back-donation in lengthening the N_α–C_β bond. Molecules used for such a comparison contain metal atoms that, even though they are isoelectronic, have significant different Pauling electronegativity values (Ru, 2.2; Fe, 1.8);[26] however, we can reasonably assume that the higher relative tendency of Ru to accept charge through the $\pi_2 \rightarrow$ Ru′ interaction in V and VI is partially offset by the higher relative tendency of the Fe atom to back-donate in I.[27]

In relation to the analysis of the Fe–(C_4H_4) interaction (point ii), we cannot describe the bonding scheme within the metalla-

(20) Considering each CO group as a 2e donor, R-DAB as a 4e donor, and C_4H_4 as a σ-C, σ-C′, η^2-C=C, η^2-C=C′ 6e donor, we have 16e around Fe and 18e around Fe′.

(21) Cotton, F. A. *Prog. Inorg. Chem.* **1976**, *21*, 1.

(22) (a) Sidgwich, N. V. *Chem. Ind.* **1927**, *46*, 799. (b) Sidgwich, N. V. *Chem. News J. Ind. Sci.* **1927**, *135*, 161. (c) Sidgwich, N. V. *Chem. News J. Ind. Sci.* **1927**, *135*, 177.

(23) M→π_3 back-donation fills up an antibonding N_α–C_β orbital (C_β–C_β bonding), while $\pi_2 \rightarrow$ M donation depopulates a bonding N_α–C_β orbital (C_β–C_β antibonding). Both mechanisms concur with the lengthening (shortening) of the N_α–C_β (C_β–C_β) bond.

(24) Keijsper, J.; van der Poel, H.; Polm, L. H.; van Koten, G.; Vrieze, K.; Seignette, P. F. A. B.; Varenhorst, R.; Stam, C. H. *Polyhedron* **1983**, *2*, 1111.

(25) (a) Staal, L. H.; Polm, L. H.; Vrieze, K.; Ploeger, F.; Stam, C. H. *J. Organomet. Chem.* **1980**, *199*, C13. (b) Staal, L. H.; van Koten, G.; Vrieze, K.; Ploeger, F.; Stam, C. H. *Inorg. Chem.* **1981**, *20*, 1830. (c) Keijsper, J.; Polm, L.; van Koten, G.; Vrieze, K.; Abbel, G.; Stam, C. H. *Inorg. Chem.* **1984**, *23*, 2142.

(26) Johnson, B. F. G.; Lewis, J. *Adv. Inorg. Chem. Radiochem.* **1981**, *24*, 225.

(27) A theoretical and experimental investigation of the electronic structure of $Fe_2(CO)_4$(R-DAB)(μ-HC≡CR) is in progress in our laboratory in order to decide this matter.

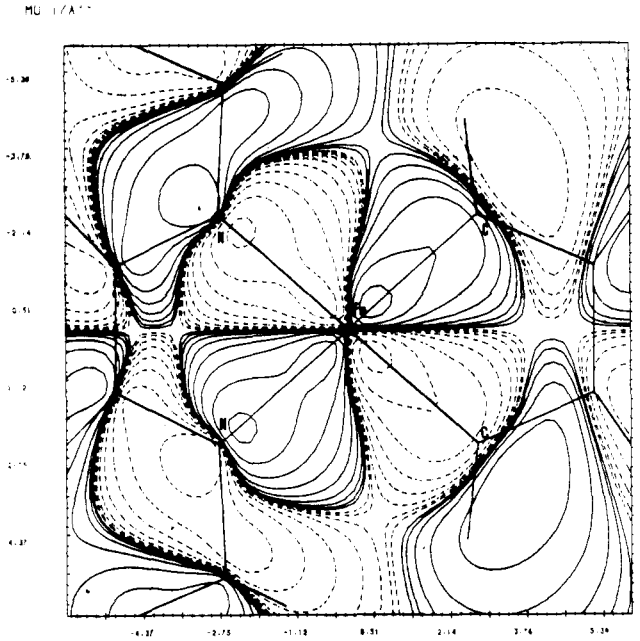

Figure 3. DV-Xα contour plot for the 17a″ MO 1 au above the *xy* plane.

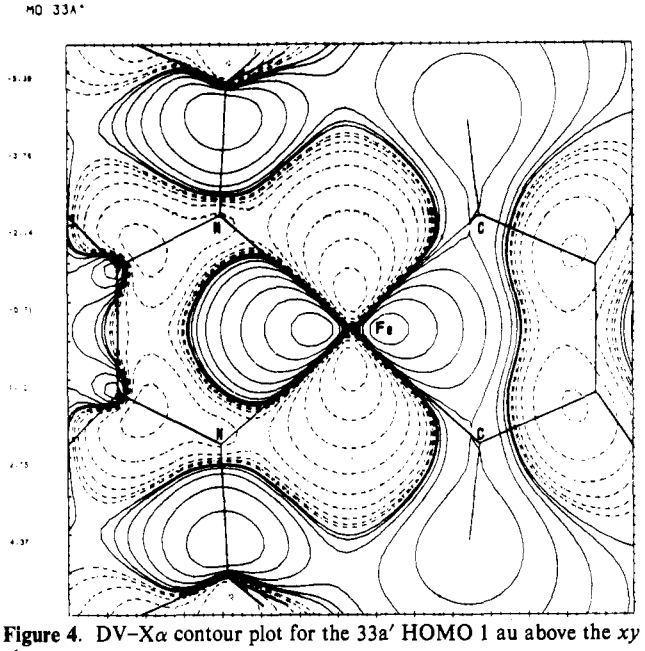

Figure 4. DV-Xα contour plot for the 33a′ HOMO 1 au above the *xy* plane.

cyclopentadienyl unit as done in ref 10, where it was connected to that of a cyclopentadienyl anion perturbed by the presence of a heteroatom fitted up with d AO's. Actually, the significant deviations from planarity of the Fe–(C_4H_4) unit[28] and the absence of an *effective* Fe′→Fe dative bond prevent, in relation to both electronic[10a] and structural demands, the possibility of describing the electronic structure of the (DAB)(CO)Fe(C_4H_4) moiety in terms of a 6-π-electron metalla aromatic ring.[10a,29-31] Nevertheless, the Fe → π_3* interaction is quite strong (see in Table I the high mixing present in the 31a′ MO between metal-based and C_4H_4 AO's), as well as the interaction with n⁻ linear combinations of C_α radical lobes, which is accounted for by the 17a″ MO (see Figure 3).

If we turn our attention now to point iii, once again the comparison with theoretical results relative to those of IV[10a] is very fruitful. The strength of Fe′–C_α and Fe′–C_β interactions is substantially the same in both cases,[32] confirming what has already been proposed in discussing point i; i.e. the substitution of two terminal carbonyls with the R-DAB ligand principally affects the MO's mainly localized on the metal atom to which the R-DAB is directly bonded. As a matter of fact, it is relevant to point out the poorer involvement of Fe′ in the 27a′ MO, which represents the C_4H_4-based π_1 level, at variance with the case for IV.[10a] Such an effect is in accord with the mentioned absence of an *effective* Fe′→Fe dative bond, which allowed in IV a high mixing of Fe′ AO's with the C_4H_4-based π_1 level as a consequence of the +1 formal charge carried by Fe′.[21]

The Fe–Fe′ interaction (point iv) is the most delicate point of the whole bonding scheme, and for this reason, before discussing it, we want to mention here some important points that are of value for an easier discussion of the forthcoming results.

According to Hoffmann's suggestion,[29,30] the $M(CO)_3$ fragment "remembers its octahedral parentage", so that its metal-based orbitals can be labeled as e_g and t_{2g} like. The higher lying e_g set accounts for the M–CO antibonding interaction, while the inner t_{2g}-like set consists of strongly metal-localized orbitals. When two $M(CO)_3$ fragments are allowed to interact to give rise to the $M_2(CO)_6$ unit, bonding and antibonding combinations with respect to the M–M interaction are obtained. Furthermore, as one passes from the $M_2(CO)_6$ unit to the real complex $M_2(CO)_6$(ligand), the e_g set is significantly involved in the metal–ligand interactions.[30,31] A large number of experimental and theoretical contributions dealing with the electronic structure of these dimers has been published.[33] Among them, several papers have been devoted to the investigation of the bonding scheme of IV, within both the MO and VB approaches.[10a,b,21,30,31] These approaches describe quite differently the Fe–Fe′ interaction in IV: the MO treatment indicates that the direct M–M bond is accounted for by the e_g-like HOMO (the t_{2g} set does not contribute as a whole to the M–M interaction), while the VB one assumes the presence of an Fe′→Fe dative bond[21] to allow the fulfillment of the EAN rule[22] for both iron atoms.

The application of qualitative theoretical arguments to the analysis of the Fe–Fe′ bond in I would suggest something very similar to what is found in IV. In contrast, this interaction is definitely different in the two cases and, more generally, different with respect to that for the $M_2(CO)_6$(ligand) complexes.[10a,b,30,31,33] Actually, among the seven MO's strongly localized on the metal centers (six t_{2g} like plus one e_g like),[34] only the 30a′ MO contributes with a positive Fe–Fe′ OP (0.024e). Moreover, it is worthwhile to mention that the highest contribution to the Fe–Fe′ bond comes from the inner ligand based 28a′ MO (0.081e). Incidentally, such a high contribution has the eventual effect of equalizing the total Fe–Fe′ OP in I and IV.[10a] Quite unexpectedly, MO's 32a′ and 31a′, which apparently should be the best candidates to account for the direct M–M bond (at least in relation to their symmetry and to the high sharing of electronic charge between metal atoms (see Table I)), contribute negatively to it; in contrast, they are strongly involved in the interaction with R-DAB and C_4H_4, respectively.[35] Another important difference with respect to the $M_2(CO)_6$(ligand) electronic structure is the nature of the HOMO.

(28) The Fe atom lies 0.236 Å above the C_4H_4 planar moiety and 0.15 Å below the N atoms; moreover, the plane containing the R-DAB ligand forms an angle of ~21° with the *xy* plane.
(29) Thorn, D. L.; Hoffmann, R. *Nouv. J. Chim.* **1979**, *3*, 39.
(30) Thorn, D. L.; Hoffmann, R. *Inorg. Chem.* **1978**, *17*, 126.
(31) (a) Trogler, W. C.; Curtis, E. J.; Ellis, D. E. *Inorg. Chem.* **1981**, *20*, 980 and references therein. (b) Gross, M. E.; Trogler, W. C.; Ibers, J. A. *J. Am. Chem. Soc.* **1981**, *103*, 192.
(32) The OP's of Fe′–C_α a′ and a″ in symmetry in I (IV) are 0.10e (0.10e)[10a] and 0.09e (0.09e),[10a] respectively while the Fe′–C_β ones are −0.15e (−0.17e)[10a] and 0.03e (0.03e).[10a]
(33) Granozzi, G.; Casarin, M. In *Topics in Physical Organometallic Chemistry*; Gielen, M., Ed.; Freund: in press; Vol. 3, and references reported therein.
(34) Both metal atoms are formally in their zero ion state, but for both of them a charge of ~+1 is eventually computed (see Table IV).
(35) MO's 32a′ and 31a′ have, among MO's strongly localized on the metal atoms, the highest OP with R-DAB and π_3* of C_4H_4 (0.08e for both).[36]
(36) Despite the low symmetry of the molecular systems, it is still possible for the C_4H_4 moiety to discriminate between MO's mainly π and σ in character. The same does not hold for R-DAB, since its bending with respect to the C_4H_4 plane (*xy* in our framework) allows extensive mixing of π and σ ligand-based MO's.

In the present case, the HOMO no longer represents the direct M–M bond[10a,b,30,33] but one among the Fe-localized d pairs ($d_{x^2-y^2}$ in our framework; see Figure 4) strongly destabilized by interaction with the R-DAB and C_4H_4 occupied MO's. Deviations from planarity of the Fe(R-DAB)(C_4H_4) fragment[28] could be ascribed, beyond crystal-packing effects, also to the possibility of weakening such a destabilizing interaction. As a whole, the Fe–Fe′ interaction is dominated by the absence of the Fe′→Fe dative bond invoked by Cotton[21] in the isoelectronic IV. The reason for such an absence has been already discussed in describing the Fe–(R-DAB) interaction.

In order to rationalize Mössbauer data, XPS spectra (vide infra), and some troublesome structural features of IIa–c, it is of relevance to know the main effects of R-DAB coordinated to Fe′, as in IIa–c (see Figure 1). Thence, a ground-state DV–Xα calculation on the model molecule $Fe_2(CO)_4$(R-DAB)(C_4H_4), containing the Fe′(CO)(R-DAB) moiety, has been also run. This calculation gives us the possibility of understanding how the new coordination site of R-DAB modifies the bonding scheme proposed for I. The most important feature of the electronic structure of this model is the presence of an *effective* Fe′→Fe dative bond (see in Table IV the high Fe–Fe′ OP). Actually, in the present case among the seven metal-localized MO's (33a′, 22a″, 32a′, 31a′, 30a′, 21a″, 29a′ MO's) only the HOMO and the SHOMO (second highest occupied MO) contribute negatively to the Fe–Fe′ bond. The presence of this strong interaction between the metal atoms is easily understood by making reference to the electronic effect of R-DAB (previously discussed) and to the relative electronegativity of Fe in II-like compounds being higher than that in I.[37] Such considerations are extremely important in understanding the peculiar behavior of the (semi)bridging carbonyl and C–C bond length differences within the C_4 organic chain in II-like compounds and in III.[11]

The key in rationalizing the significant variations of the Fe′–$(CO)_{sb}$ (sb = semibridging) bond angle along the investigated series is the strength of the Fe–Fe′ bond. In I, the (n^+, n^-) → Fe donation is strong enough to avoid the presence of an *effective* Fe′→Fe bond; nevertheless, Fe needs to redistribute its charge excess by back-donating into the π_3^* C_4H_4 level (see above) and into the $\pi_\parallel^*$ level (∥ refers to the plane passing through the iron atoms and the carbonyl itself) of the $(CO)_{sb}$ bonded to Fe′ but pointing toward Fe (see Figure 1).[38] Such a back-donation into $\pi_\parallel^*$ allows us to understand the significant deviation from linearity of the Fe′–$(CO)_{sb}$ angle (164.4°).[11,39]

In II-like compounds a strong Fe–Fe′ interaction is present and a significant amount of charge is transferred from Fe′ to Fe. The troublesome behavior of the semibridging carbonyl, whose Fe′–$(CO)_{sb}$ angle ranges from almost linear in IIc (171.7°)[11] to semibridging in a II-like compound with R = phenyl (Ph) (164.4°),[11] can be explained in terms of the electronic properties of the substituents on the C_4 organic chain. In IIc two strong electron-withdrawing C(O)OMe substituents are present, so that the back-donation into the C_4-based π_3^* level is favored with respect to that into $\pi_\parallel^*$. This gives rise to an almost linear carbonyl. In the II-like compound with R = Ph, a semibridging carbonyl is present because the C_4 chain is now less disposed to accept charge into its π_3^* level. By using similar arguments, one can also explain the asymmetrically bridging coordination of a CO group in III (see Figure 1). Here the Fe–Fe′ interaction should not be very strong (as in I) and nitrogen-induced charge accumulation on Fe cannot be redistributed by back-donating into the R-DAB π_3^* level because of its particular structural arrangement (R-DAB substitutes two CO groups, one perpendicular to the *xy* plane and the second in the *xy* plane). The only active charge redistribution mechanisms are back-donations into C_4R_4 π_3^* and CO $\pi_\parallel^*$ levels.

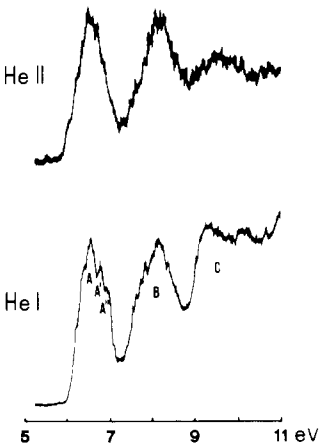

Figure 5. He I (bottom) and He II (top) PE spectra of I.

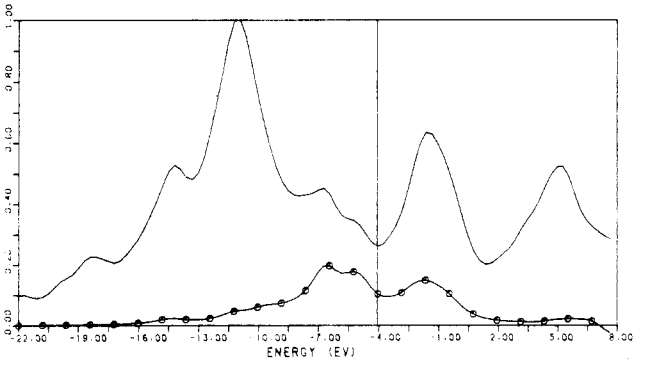

Figure 6. Total and partial density of states for I. The PDOS (Fe + Fe′; –O–) is scaled to the total DOS (—).

The presence of a subtle back-donation balance into virtual orbitals of the C_4 organic chain and of the semibridging carbonyl is confirmed by the peculiar trend showed by the C_α–C_β (C_β–C_β) bond lengths: in IIc C_α–C_β = 1.41 Å and C_β–C_β = 1.44 Å;[11] in a II-like compound with R = Ph C_α–C_β = 1.37 Å and C_β–C_β = 1.45 Å;[11] in III C_α–C_β = 1.45 Å and C_β–C_β = 1.41 Å.[11] Bond length values for IIc and III clearly indicate an extensive population of the C_4-based π_3^* level, at variance with the case for the II-like compound with R = Ph, where the poorer population of the π_3^* orbital gives rise to significantly different C–C bond lengths.

UV-PES Results. The He I/He II PE data of I are reported in Figure 5. The experimental pattern in the low-IE region (up to ~9 eV) is dominated by the presence of two structured bands, namely A and B centered at 6.6 and 8.2 eV, respectively. TSIE calculations[15] (Table I) reproduce this trend very well, in relation to relative intensities and position of bands. Absolute IE values are, however, uniformly overestimated by ~1 eV.

When we continue with the analysis of the spectral pattern, it is evident (see Figure 5) that band A has a lower intensity than band B. On this basis, the former is assigned as a whole to three ionization events (33a′, 22a″, 32a′ MO's), while band B is assigned to the ionization from the following four MO's (31a′, 21a″, 30a′, 29a′). It is noteworthy that band A includes ionizations only from Fe-based MO's, while band B includes those only from Fe′-based levels. In this regard one can make reference to the total and partial DOS (see Figure 6), which shows, in the lowest IE region of occupied levels, the presence of two bands mainly due to Fe- and Fe′-localized MO's with a relative intensity ratio similar to the experimental one.

Relying on TSIE ordering, we could relate the lower IE side of band A to the ionization from the 33a′ HOMO while A′ and the shoulder A″ should be assigned to the ionization from 22a″ and 31a′ MO's, respectively. The decrease in relative intensity of the higher IE side of band A as one passes from the He I to

(37) One has to remember that, in II-like compounds, Fe is more electronegative than Fe in I, having three CO groups in its coordinative shell.
(38) In the title molecules the geometry is always nonsawhorse,[30] with a carbonyl bonded to Fe′ but pointing toward Fe.
(39) (a) In 1965 Kettle proposed on the basis of symmetry arguments that the deviation from a linear M–C–O structure is a function of the difference in occupation of the two π^* orbitals.[39b] (b) Kettle, S. F. A. *Inorg. Chem.* **1965**, *4*, 1661.

Table V. Core Level Binding Energy Values (eV)

	Fe $2p_{3/2}$			
	Fe	Fe′	fwhm	N 1s
free ligand				399.6
$Fe(CO)_2(NO)_2$	709.7[a]			
$Fe(CO)_5$	709.8[a]			
$Fe(CO)_3(\eta^4\text{-}C_4H_6)$	709.1[b]			
I	708.5	709.6	3.1	400.3
IIc	708.8	709.7	2.5	400.3
III	709.1	709.7	2.2	400.3

[a] From ref 45a. [b] From ref 45b.

He II source (see Figure 5) is in accord with such an assignment.[40] The TSIE ordering seems to be experimentally verified also for band B. Actually, the lower IE side of band B suffers an evident relative intensity decrease on passing to the more energetic radiations (see Figure 5), in agreement with the high localizaton of the 31a′ MO on the C_4H_4 moiety.[40]

The broad and unresolved band envelope C beyond 9 eV shows a dramatic decrease in relative intensity on switching to the He II radiation. This is then assigned with confidence to ligand-based MO's.[40] Tentatively, we would associate it with the ionizations from 20a″, 19a″, 18a″, and 28a′ MO's.[42] Among these MO's, those strongly reminiscent of free-ligand levels are the 20a″ and 18a″ MO's, which correspond to the C_4H_4-based π_2 level and to the in-phase linear combination of C_4H_4/R-DAB n^- levels.[43] An extensive rehybridization, favored by the nonplanarity of the (R-DAB)–Fe–(C_4H_4) unit, prevents a similar assignment for 19a″ and 28a′ MO's.

Ionizations from inner MO's reported in Table I are hidden under a broad and unresolved band, centered at 13.5 eV (not reported in Figure 5), which is also due to ionizations from iron–CO σ-bonding MO's and 1π and 4σ CO-localized levels. The analysis of this region is unproductive and is out of the scope of this contribution.

As far as PE data relative to IIa–c and III are concerned, an extensive decomposition in the ionization chamber prevented the recording of reproducible spectra.

XPS Results. The core level binding energy values (BE's) of the constituent elements of the investigated compounds are reported in Table V together with energy values of other compounds chosen as references.

The increase of the N 1s BE in coordinated R-DAB (400.3 ± 0.2 eV) with respect to that of the free ligand (399.6 ± 0.2 eV) is in agreement with a decrease of the electronic density over the N atoms as a consequence of coordination. Furthermore, the analysis of the iron $2p_{3/2}$ photoelectronic peaks and relative values of the fwhm (full width at half-maximum) in I, IIc, and III agrees with the presence of two nonequivalent iron atoms. The relative BE's have been obtained by deconvoluting the Fe $2p_{3/2}$ bands and are reported in Table V. In the forthcoming discussion the assignment of XPS bands will be carried out by making reference to literature data for related compounds[44] as well as to results of the reported theoretical calculations.

For I, the component of 709.6 eV (Table V) is assigned to the ionization of the Fe′ $2p_{3/2}$ core level by making reference to the iron $2p_{3/2}$ BE in $Fe(CO)_5$, $Fe(CO)_2(NO)_2$, and $Fe(CO)_3(\eta^4\text{-}C_4H_6)$ (709.8, 709.7, and 709.1 eV, respectively).[44] The second component at 708.5 eV indicates a slightly higher electron density for Fe than for Fe′ as a consequence of the substitution of two CO ligands by the R-DAB ligand.

In IIc, according to theoretical calculations, the two components at 708.8 and 709.7 eV should be associated with the ionization of the $2p_{3/2}$ core level of Fe and Fe′, respectively. Actually, the iron $2p_{3/2}$ BE of Fe in II would be expected to have the same value as for Fe′ in I (709.6 eV); however, the presence of an *effective* Fe′→Fe dative bond (vide supra) with a significant charge transfer from Fe′ to Fe explains the shift toward lower binding energy of

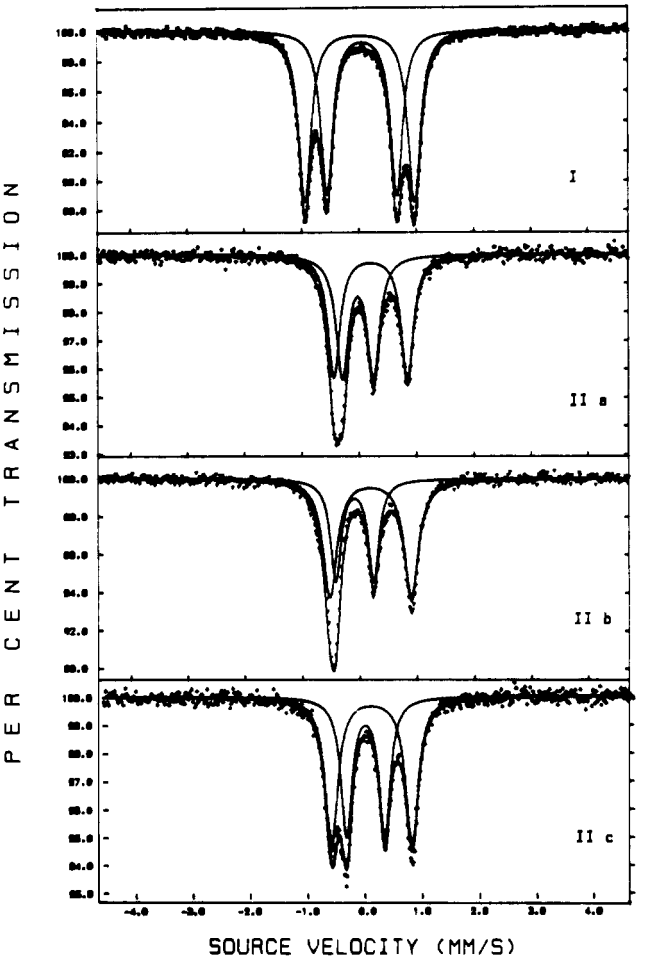

Figure 7. Mössbauer-effect spectra of compounds I and IIa–c at 77 K.

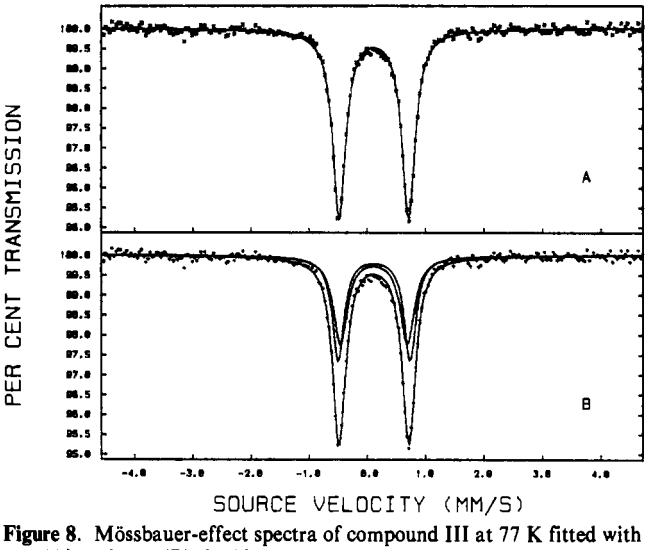

Figure 8. Mössbauer-effect spectra of compound III at 77 K fitted with one (A) and two (B) doublets.

(40) In fact, on the basis of the Gelius model,[41a] we expect a marked decrease in the cross section ratio σ(C 2p)/σ(Fe 3d) on passing from the He I to the He II excitation source.[41b]

(41) (a) Gelius, U. In *Electron Spectroscopy*; Shirley, D. A., Ed.; North-Holland: Amsterdam, 1972; p 311. (b) Rabalais, J. W. In *Principles of UV Photoelectron Spectroscopy*; Wiley-Interscience, New York, 1977.

(42) This assignment has been done by keeping in mind the uniform shift of ~1 eV between experimental and theoretical IE's. The onset of band C is at ~9 eV, and it covers an energy range of ~1.5 eV. On this basis it should include ionizations from 20a″, 19a″, 18a″, and 28a′ MO's.

(43) The main character of the MO's has been assigned by making reference to relative CP's.

(44) (a) Barber, M.; Connor, J. A.; Guest, M. F.; Hall, M. B.; Hillier, I. H.; Meredith, W. N. E. *Faraday Discuss. Chem. Soc.* **1972**, *54*, 219. (b) Eekhof, J. H.; Hogeveen, H.; Kellog, R. M.; Sawatzky, G. A. *J. Organomet. Chem.* **1976**, *111*, 349.

Table VI. Mössbauer Data for I, IIa–c, III, IV,[12a–c] and VII[12d,e]

	T, K	δ, mm s^{-1}	ΔE_q, mm s^{-1}	Γ, mm s^{-1}	A, %
I	77	0.009 (1)	1.909 (4)	0.25	52.2
		0.047 (2)	1.221 (3)	0.24	47.8
IIa	77	0.197 (3)	1.279 (5)	0.25	50.4
		−0.025 (3)	0.545 (4)	0.25	49.6
IIb	77	0.184 (3)	1.420 (6)	0.29	60.1
		−0.095 (3)	0.663 (4)	0.22	39.9
IIb	room temp	0.118 (8)	1.396 (16)	0.28	60.3
		−0.131 (6)	0.701 (11)	0.23	39.7
IIc	77	0.108 (2)	1.420 (3)	0.26	55.0
		0.004 (3)	0.679 (5)	0.23	45.0
III	4.2	0.115 (4)	1.256 (9)	0.22	50.0[b]
		0.118 (6)	1.140 (12)	0.24	50.0[b]
III	77	0.116 (3)	1.238 (9)	0.25	50.0[b]
		0.111 (3)	1.154 (12)	0.29	50.0[b]
III	room temp	0.035 (2)	1.167 (4)	0.26	100.0
IV[12a–c]		−0.02	1.23		
		−0.10[a]	1.38[a]		
VII[12d,e]		0.02	1.46		

[a] Calculated from Figure 1 in ref 12c. [b] Values constrained by the fitting procedure.

the iron $2p_{3/2}$ component associated with Fe.

For III, the two iron $2p_{3/2}$ components are very close in energy (709.1 and 709.7 eV). Consistent with the assignment for I and with the arguments reported in Theoretical Results, the 709.7-eV component is assigned to Fe′. Furthermore, the close similarity experimentally found for the two Fe $2p_{3/2}$ values suggests the presence of very efficient charge redistribution effects. There is no doubt that a leading role in such a redistribution is played by the asymmetrically bridging carbonyl.

Mössbauer Results. The Mössbauer-effect spectra of compounds I and II and of compound III are reported in Figures 7 and 8, respectively. The spectra of I and IIc consist of four lines of roughly equal intensities corresponding to two quadrupole-split doublets assignable to two distinct iron sites. In contrast, the spectra of compounds IIa,b consist of three lines of intensity 2:1:1 that can again be fitted to two doublets, with overlap of the low-velocity components. The existence of two different iron sites is fully consistent with the stoichiometry and the crystal structure[11] of the title compounds.

The first problem to be addressed is the assignment of the individual lines to a specific quadrupole doublet. The criterion we followed has been that of minimizing the range of the possible isomer shift values by adopting a nested-doublets configuration. This is supported both by theoretical results[45] (see Tables I and IV) and by comparison with the calculated isomer shifts and quadrupole splitting values pertaining to other related cluster compounds (see Table VI).[12]

The second problem we need to confront deals with the assignment of a single quadrupole doublet to a specific iron site in the complexes. The solution of this problem again involved theoretical results[45] and comparison with the Mössbauer spectrum of IV.[12a–c] In this regard, it has to be noted that only one value for the isomer shift and quadrupole splitting is reported in the literature,[12a–c] without any indication to which iron site it refers to. The comparison of quadrupole splitting values of I and IV (see Table VI) indicates that one iron atom has the same ΔE_q value in both complexes. Keeping in mind the surrounding of the iron atoms (see Figure 1), it is quite obvious to assign (not only in I but also in IV) the quadrupole doublet with ΔE_q values of 1.221 (3) mm s^{-1} in I and 1.23 mm s^{-1} in IV to the Fe′ atom, i.e. the iron π-bonded to the C_4H_4 moiety. Such an assignment is confirmed by the agreement existing between δ values (see Table VI) and quantum-mechanical calculations for I, which eventually determined a higher (smaller) 3d (4s) occupation number for Fe′.[45]

The assignment of the quadrupole doublets for the Mössbauer spectra of IIa–c is more troublesome and has been carried out by making reference to the electronic consequences of the presence of a strong Fe–Fe′ bond in II-like compounds. The existence of this strong interaction gives rise to a significant charge transfer from Fe′ to Fe with a strong involvement of the Fe′ d AO's (one has to remember that, in the II-like compounds, among the seven metal-based MO's, only the HOMO and the SHOMO contribute negatively to the Fe–Fe′ bond). The consequent increase in the d-electron density of Fe compared to that in Fe′ should change its isomer shift in the same direction. Therefore, we expect δ values for Fe′ much lower than for Fe in IIa–c, as already found in I. On this basis, we propose to assign the first doublets in Table VI to the Fe site. The variations observed among the three compounds may well be attributed to the different electronic properties of the substituents in the C_4 chain. The corresponding ΔE_q values (1.279, 1.420, and 1.420 mm s^{-1}) are consistent with the value calculated for the Fe site in IV (1.38 mm s^{-1}). As far as the Fe′ values are concerned, the isomer shift decreases with respect to that of I are as expected; the much lower values of the quadrupole splitting are rather surprising and might be ascribed to a better balance between the lattice and the electronic contributions.

The Mössbauer-effect spectrum of compound III, obtained at 77 K, is characterized by the presence of two single lines whose width is narrow enough to indicate the presence of only one quadrupole doublet. In order to check the accidental degeneracy of ΔE_q as well as δ values for Fe and Fe′ sites, compound III was synthesized again. The purity of the sample was checked by IR and ^{1}H NMR measurements. Moreover, a further solid-state X-ray data collection was carried out, confirming literature results.[11] The relative Mössbauer-effect spectra, obtained at room and liquid-helium temperatures, reproduced that already collected at 77 K. However, while at the highest temperature any attempt to fit the spectrum with two separate doublets failed, the spectra at 77 and 4.2 K can be fitted to two doublets with the same isomer shift but with values for the quadrupole splitting clearly outside the experimental error (see Table VI). Both fitting procedures give very good χ^2 values, but we prefer the two-doublet analysis on a chemical basis. In fact, while on one side theoretical considerations predict substantial identity of the electronic configurations for the two iron centers, on the other side it is extremely difficult for the electric field gradient of the two iron sites to have the same values in all the investigated temperature ranges.

Conclusions

Theoretical data indicate that, quite counterintuitively with respect to qualitative electron-counting methods, the coordination of the R-DAB ligand to a different metal center significantly modifies the overall bonding scheme of the investigated molecules. Moreover, they allow a rationalization of peculiarities of crystallographic data on the basis of a subtle balance of back-bonding into virtual orbitals of R-DAB, of the C_4H_4 chain, and of the (semi)bridging CO. Finally, as a whole, they point out once more that the metal–ligand interactions are significantly influenced by the strength of the metal–metal bond. Both XPS and Mössbauer experimental data indicate a strong delocalization of charge, which is extremely efficient in III. The comparison between experimental results and theoretical outcomes is very good, in particular taking into account the complexity of the investigated molecules. This confirms that the DV–Xα method is "head and shoulders" above any other computational technique for obtaining quantitative information about the bonding schemes of very complex molecular systems.

Acknowledgment. Thanks are due to G. Cossu, G. Righini, and F. De Zuane for their invaluable technical assistance.

Registry No. I, 122423-79-4; IIa, 122423-80-7; IIb, 122423-81-8; IIc, 122423-82-9; III, 122423-83-0; Fe(Me-DAB)CO, 122423-84-1; Fe(CO)$_3$, 52491-41-5.

(45) Theoretical results indicate very similar electronic charges for both iron atoms; slight differences are relative to orbital occupation numbers.